Plastisols of Poly(vinyl Chloride); Particle Size Distribution, Morphology, Rheology, and Mechanism of Aging*

N. NAKAJIMA and C. A. DANIELS, *BFGoodrich Chemical Division Technical Center, Avon Lake, Ohio 44012*

Synopsis

Plastisols of poly(vinyl chloride) (PVC) are suspensions of fine resin particles in plasticizer with about a 50% resin volume fraction. Typically, the gross particle size ranges from about 15 to 0.2 μm and smaller, where the common practice of spray drying these resins dictates that the size ranges include agglomerates as well as the ultimate particles. In this work we have related the particle size distribution to the dynamic mechanical behavior with model plastisols prepared from various particle-size fractions of a commercial resin. This relationship, together with the microscopic observation of the particle dispersions, provided an interpretation of the plausible mechanisms of the viscoelastic response. The morphological observation of the particle aggregates, the changes of the particle size distribution during the aging, and the above viscoelastic study have established that deagglomeration is the dominant cause of the increase of viscosity during aging.

INTRODUCTION

The plastisol of poly(vinyl chloride) (PVC) is a suspension of fine resin particles in a plasticizer.[1a] Typically, the gross particle size ranges from about 15 to 0.2 μm and smaller.[1b] Since commercial plastisol resins are spray dried and ground, this size range includes agglomerates as well as the ultimate particles.[1b]

The commercial applications of these plastisols are for coatings, films, sheets, foams, and rotational casting,[1c] where the material is first spread out and then heated to a gel and fused.[1d] The importance of rheology in the processing behavior has been recognized.[1e,2,3] At room temperature it exhibits thixotropic behavior, as well as shear thinning at low shear rates, and exhibits dilatant behavior at high shear rates. Rheological study has hitherto been limited to the shear flow measurements.[4] The present study is a measurement of sinusoidal stress–strain behavior at a small deformation. This enables us to observe the behavior of the system with minimum disturbance.

The effect of volume fraction of the resin particles on viscosity has drawn the attention of researchers.[4] In contrast, the effect of the particle size distribution on viscoelasticity at a fixed volume fraction has been given little attention. This is obviously of very practical importance. Whereas the behavior of spherical and monodisperse particle dispersion is of fundamental interest,[5] it is rather remote from practical systems, where differently shaped particles of varied sizes are present. These variables are taken into account in this work. The scope of this work is to characterize the viscoelastic behavior of model plastisols, relating and interpreting them on the basis of particle size, distribution, and morphology.

* Presented at the 50th Jubilee Meeting of the Society of Rheology, Boston, Massachusetts, October 28–November 1, 1979.

Journal of Applied Polymer Science, Vol. 25, 2019–2044 (1980)

0021-8995/80/0025-2019$02.60

The work is also designed to elucidate the mechanisms of the aging, which is the increase of viscosity with the time of storage.

EXPERIMENTAL

Sample Preparation

The PVC plastisol-grade resin used in these experiments was a commercial product of the BFGoodrich Chemical Division. It is designated as RF resin. The resin was fractionated by the Majac Division of the Donaldson Company, Tulsa, OK. The fractions were collected in size increment from 1 to 2 μm, and then to 4, 8, 16 μm, and larger. They are designated as 1F, 2F, 3F, 4F, and 4C, respectively. The fine-particle FF resin, was the fraction collected in the filter of the air classifier. The scanning electron micrographs were obtained on the Cambridge model S410 SEM (Cambridge Instrument Co., Monsey, NY 10952), courtesy of Case Western Reserve University.

Plastisols were prepared from RF, FF, and 4C resins by mixing the dry resin in di-2-ethylhexylphthalate (DOP) in the standard proportion of 100 parts resin to 60 parts plasticizer by weight. After aging for two weeks, blends were prepared by mixing these plastisols in various proportions. Mixing was done using laboratory-type Hobart plastisol mixers (Hobart Manufacturing Co., Troy, OH).

Determination of Particle Size Distribution

Particle-size-distribution analyses were made using the Micromeritics Sedigraph[6] (Micromeritics Instrument Co., Norcross, GA). On dry resins, the analyses were made in dibutyl sebacate. Analyses of the particle size distribution in the plastisols were made by diluting the plastisols with dibutyl sebacate. Dispersion of the dry resins in the medium of choice involved the use of ultrasonics, whereas in the case of the plastisol-based analyses, simple dilution with slow mechanical mixing was employed.

Certification of the size distribution of the resin fractions was accomplished by employing Coulter Counter procedures. These analyses, done at Majac, were verified in our laboratory by an identical method.

Observation of Morphology

The morphology of the resin fractions in their particulate form was made by mounting the samples and observing their features on the Cambridge S410 scanning electron microscope. The magnifications are listed in the captions for the respective photomicrographs, and they typically ranged from 750 to 15,000×. These magnification factors were calibrated using a grid-spacing standard.

Measurements of Dynamic Properties

The Rheometrics Mechanical Spectrometer (Rheometrics, Inc., Union, NJ) was used with 25-mm (radius) parallel disks at 1-mm gap. It was operated in a sinusoidal oscillation with strain amplitudes of 0.0350 and 0.0875, which were calculated at the periphery of the disk. The data of the complex viscosity $|\eta^*|$,

the elastic modulus G', and the dynamic viscosity η' were observed in the angular frequency range of 10^{-1} to 3×10^2 rad/sec.

RESULTS

Particle Size and Size Distribution

Deagglomeration

In order to assess the magnitude of deagglomeration of the spray-dried aggregates, fraction 4C, the coarsest particles in the distribution were monitored. The method was to prepare a fresh plastisol of the fraction, to sample it, and to measure the size distribution of the particles at set intervals. From the plastisol a sample was taken immediately after mixing, and at one day and one week from the preparation date. These were diluted and analyzed in the manner just described. As shown in Figure 1, the coarse fraction immediately changes to a coarse and fine bimodal distribution of sizes whose relative concentrations changed with time. The larger component of 4C has a median diameter of approximately 15 μm and composes about 82 mass % of the sample initially. This decreases to 78 mass % in one day and to 70 mass % in one week. The second component, whose median diameter is approximately 0.7 μm, increases in a corresponding manner, and by one week, traces of the ultrafine fraction of particles smaller than 0.36 μm are apparent. In Figure 1 the size distribution of a dispersion of the same fraction 4C is shown, prepared in a different manner than in the other three measurements. This powder dispersion was prepared at exactly the same final concentration to which the plastisol was diluted, but in dibutyl sebacate. Thus, the sample encountered a completely different environment, both in concentration and in dispersing medium. The resultant particle size distribution shows that an even greater degree of deagglomeration could be achieved from the aggregate-rich portion of the plastisol resin, such that the coarse mode of the distribution could be reduced to nearly 50 mass % of the sample.

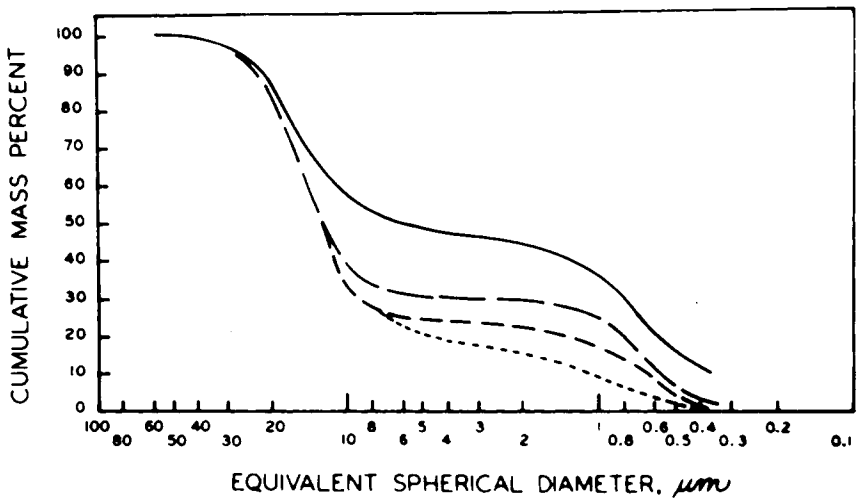

Fig. 1. Deagglomeration of aggregated particles during storage.

Clearly, with time, the resin aggregates break down and should significantly affect the rheology of the plastisols. From these data, increases in the plastisol low-shear viscosity, a commonly observed phenomenon, can be attributed, at least in part, to a deagglomeration of the spray-dried aggregates present in the resin. The degree to which this breakdown occurs depends significantly on the preparation method and on the chemical nature of the plasticizer.

Size Distribution

Shown in Figures 2–4 are particle size distributions of the component resins and the blends expressed as cumulative mass % smaller. With the blends, the solid lines are distributions calculated from those of the components and the broken lines are the observed ones.

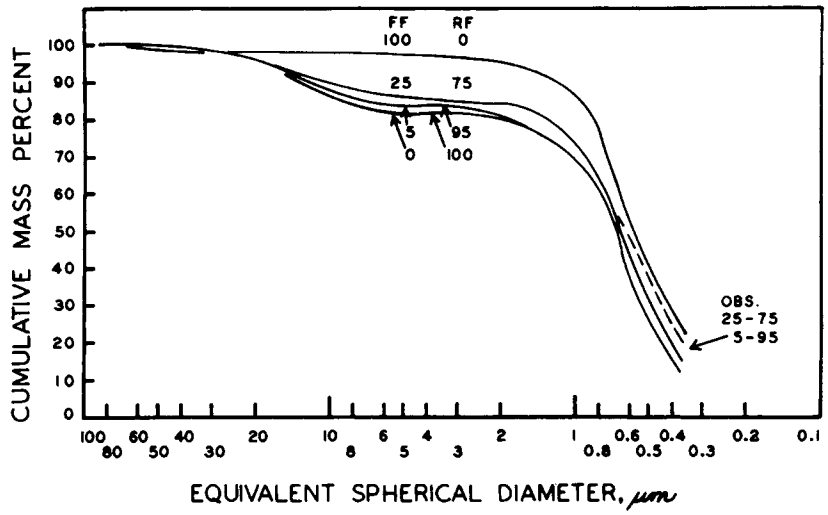

Fig. 2. Particle size distribution of FF–RF blends.

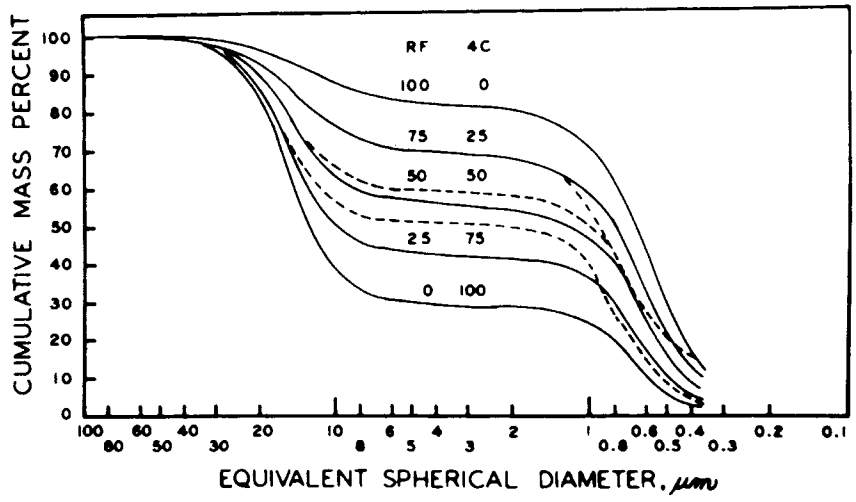

Fig. 3. Particle size disitribution of RF–4C blends.

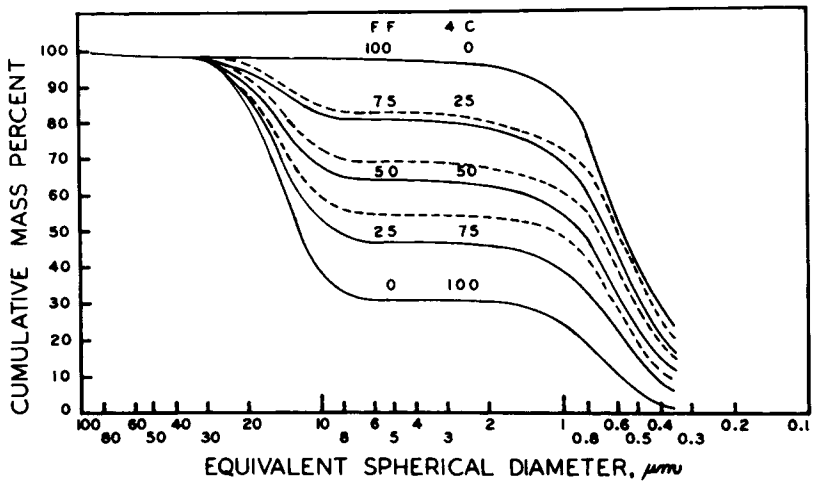

Fig. 4. Particle size distribution of FF–4C blends.

These distributions are approximately bimodal with one exception—resin FF. Therefore, we can describe them in terms of coarse and fine fractions. The particle sizes smaller than 0.37 μm were not measured because of the long times required. This fraction will be called the ultrafine.

With FF–RF blends the calculated and the observed curves agree except for the higher amounts of the ultrafines in the observed data. On the other hand, with RF–4C and FF–4C blends there are rather large discrepancies. On first glance, it appears that the data of 4C resin might be wrong. While this is still a possibility, the 4C curves calculated from the data of six blends are not in agreement with each other. It appears that during the preparation of blends some deagglomeration might have taken place, increasing the fines and ultrafines in variable amounts.

The amounts of the coarse, fine, and ultrafine fractions and the median diameters of the coarse and fine are summarized in Table I. All data were taken from the observed curves.

Morphology

Figures 5–7 show the electron microscopic photographs of FF resin and five air-classified samples at two magnifications. At 15,000× the spherical ultimate particles are observable. Also, those particles exist in three different forms—the isolated particles, the agglomerates, and the fused large particles. At the lower magnifications, it can be seen that the agglomerates and fused particles are not spherical. There are some broken particles also, which are visible in Figure 8. Note that on the surface of fraction 4C there appears some decoration with very fine particles. These no doubt are held by static forces and were difficult to separate from the more fused agglomerates in the air classification. These fine particles are probably those appearing in the initial size-distribution analysis as the smaller size mode in Figure 1. With time, these decorated surface-held particles are separated from the larger aggregate when the plasticizer medium diffuses between the contact points. Although not directly verified, the further increase in amount of fines seen in the size distribution on the aging of the

TABLE I
Particle Size Distribution

Resin (components, blends)	Mass fraction, %				Median Diam., μm	
	Coarse (>3.5 μm)	Fine, Ultrafine	Ultrafine (<0.37 μm) obsd	Ultrafine (<0.37 μm) calcd	Coarse	Fine
FF	3	97	24.5	—	15[est.]	0.66
FF–RF 25/75	15	85	20.5	15.4	13.0	0.63
FF–RF 5/95	18	82	20.5	13.2	13.5	0.60
RF	18	82	12.5	—	13.0	0.65.
FF	3	97	24.5	—	15[est.]	0.66
FF–4C 75/25	19	81	22.5	18.9	14.2	0.58
FF–4C 50/50	32	68	17.0	13.3	14.8	0.60
FF–4C 25/75	46	54	10.0	7.6	15.1	0.62
4C	70	30	2.0	—	15.1	0.73
RF	18	82	12.5	—	13.0	0.65
RF–4C 75/25	30	70	14.5	9.8	15.0	0.76
RF–4C 50/50	42	58	7.5	7.3	15.1	0.67
RF–4C 25/75	50	50	3.5	4.6	15.9	0.78
4C	70	30	2.0	—	15.1	0.73

plastisol is felt to be caused by attack on the large aggregates by the plasticizer. The reasoning for this mechanism is that observation of the surfaces of fraction 4C does not reveal enough loosely held fines to account for the nearly 30 mass % which is apparent in the size analyses after aging of the plastisol for one week.

Similar decoration can be seen in the other fractions separated from the parent resins. The major features of the resin agglomerates are consistent throughout the size fractions collected: randomly shaped aggregates varying in degree of fusion of the ultimate particles of which they are comprised, decorated at the surface with very fine single particles and smaller aggregated groups of particles.

Dynamic Properties

The amplitude dependence of the dynamic properties are shown in Figures 9 and 10. The material behavior is clearly nonlinear; viscosity and elastic modulus become lower at the higher amplitude. However, the nonlinearity of viscosity, i.e., the loss modulus, is much smaller than that of the elastic modulus so that sometimes it is hardly noticeable (Fig. 9). Henceforth, all the data presented are at the strain amplitude of 0.0350. The frequency dependence of G'' is usually a smooth curve, but that of G' gives scattered data (Fig. 10). This is typical of dispersions containing a high volume of solid particles.

Reproducibility of the measurement is shown in Figure 11, where the range of the observed data of seven runs is indicated. The runs consisted of five different charges of the sample and two repeats of the same charges. In general, G' is less well reproduced than G''. Again, this is typical of the dispersions of this type. The elasticity must be related to the packing "structure," which is constantly varying.

The lowest frequency of the observation was 10^{-1} rad/sec; the highest was

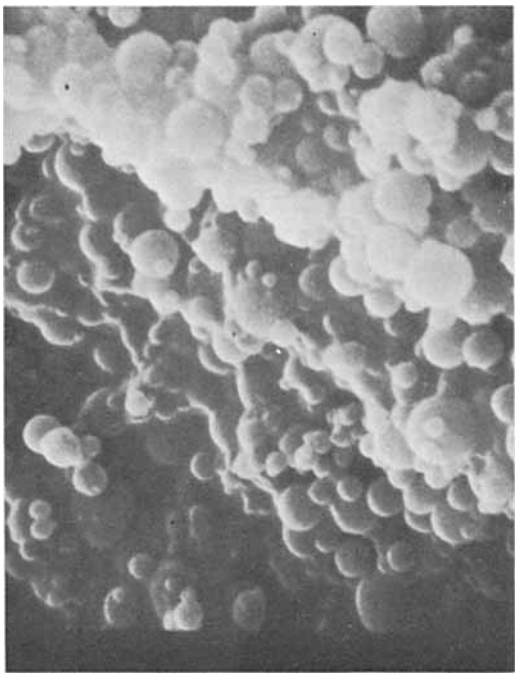

Fig. 5. SEM of fractions FF and 4C: (a) FF, 1,500×; (b) FF, 15,000×; (c) 4C, 750×; (d) 4C, 15,000×.

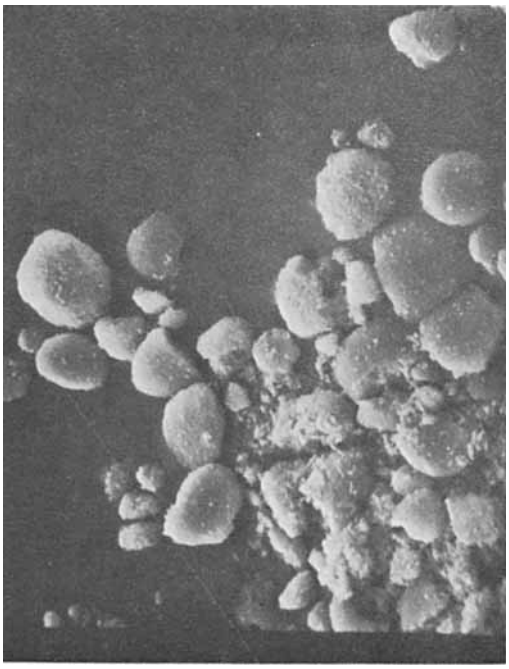

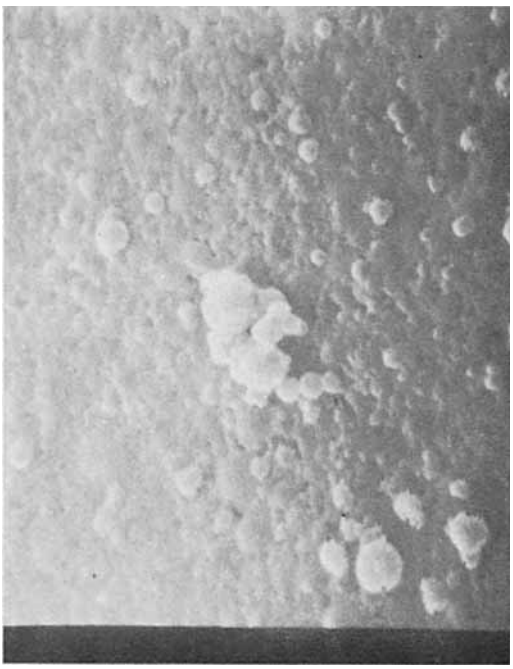

Fig. 5. (*Continued from previous page.*)

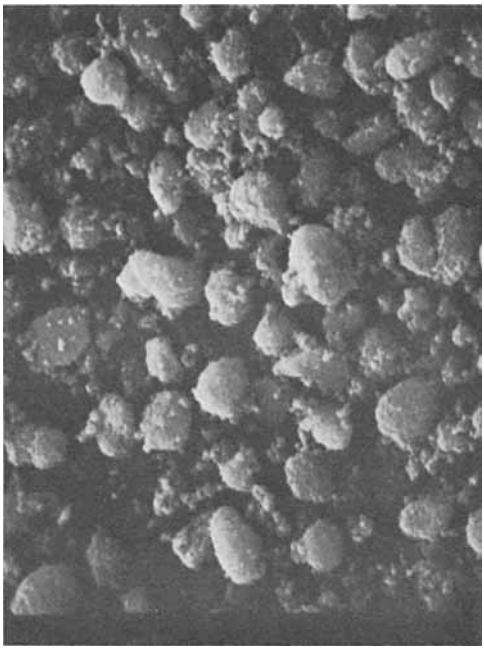

(a) 10μm

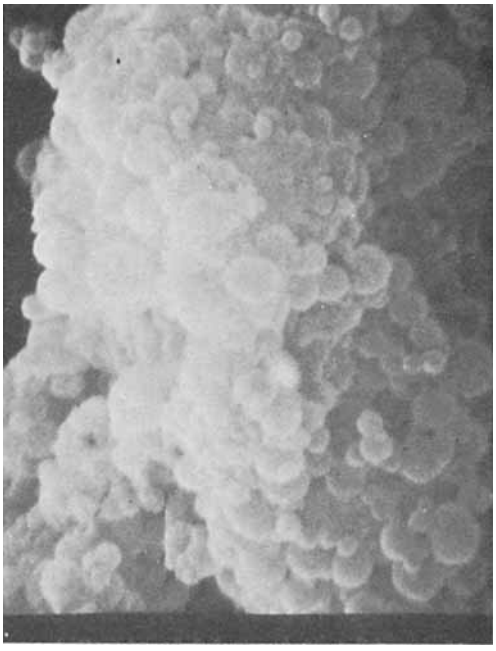

(b) 1μm

Fig. 6. SEM of fraction 3F and 4F: (a) 3F, 1,500×; (b) 3F, 15,000×; (c) 4F, 1,500×; (d) 4F, 15,000×.

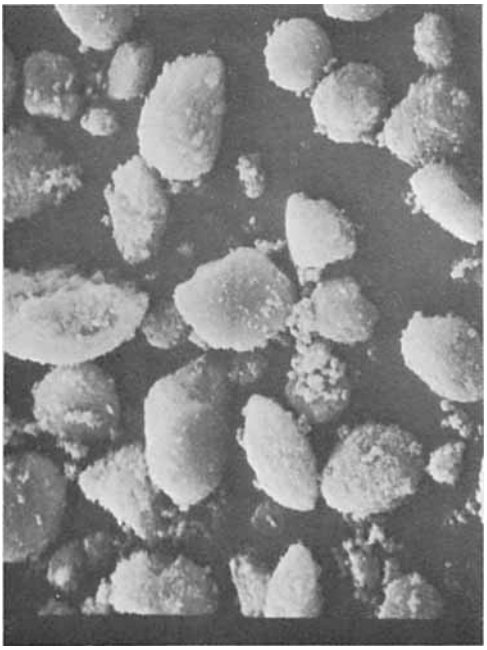

(c) 10 μm

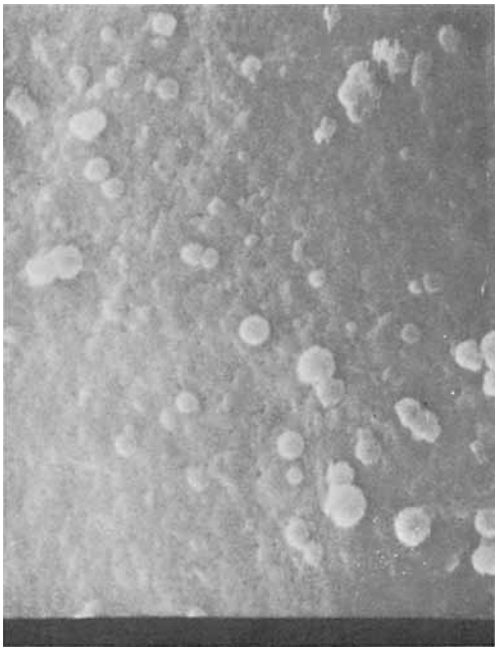

(d) 1 μm

Fig. 6. (*Continued from previous page.*)

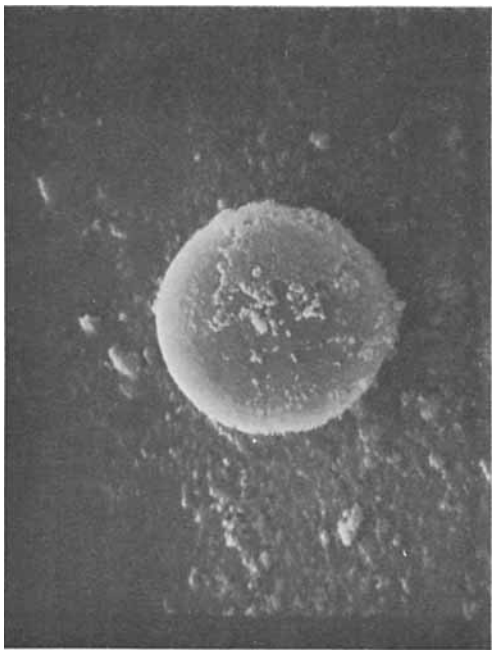

Fig. 7. SEM of fraction 1F and 2F. (a) 1F, 1,500×; (b) 1F, 15,000×; (c) 2F, 1,500×; (d) 2F, 15,000×.

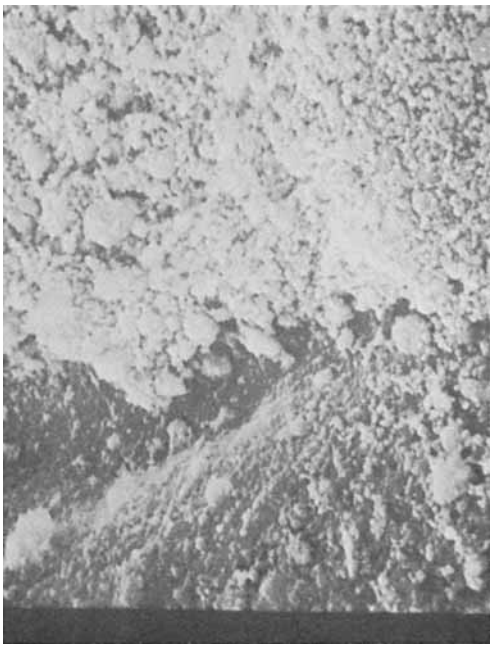

(c) 10 μm

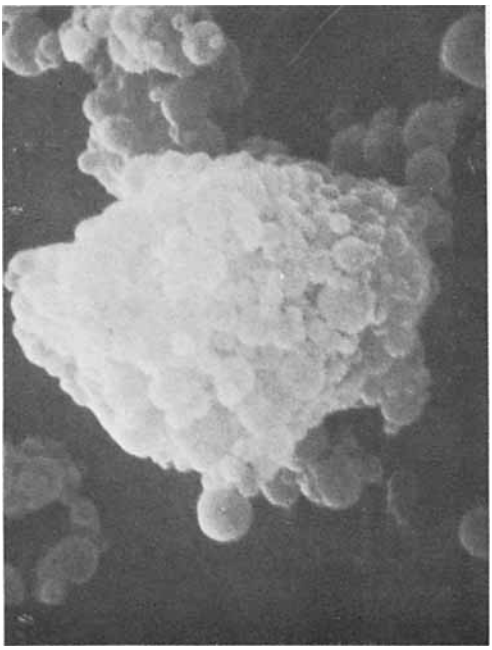

(d) 1 μm

Fig. 7. (*Continued from previous page.*)

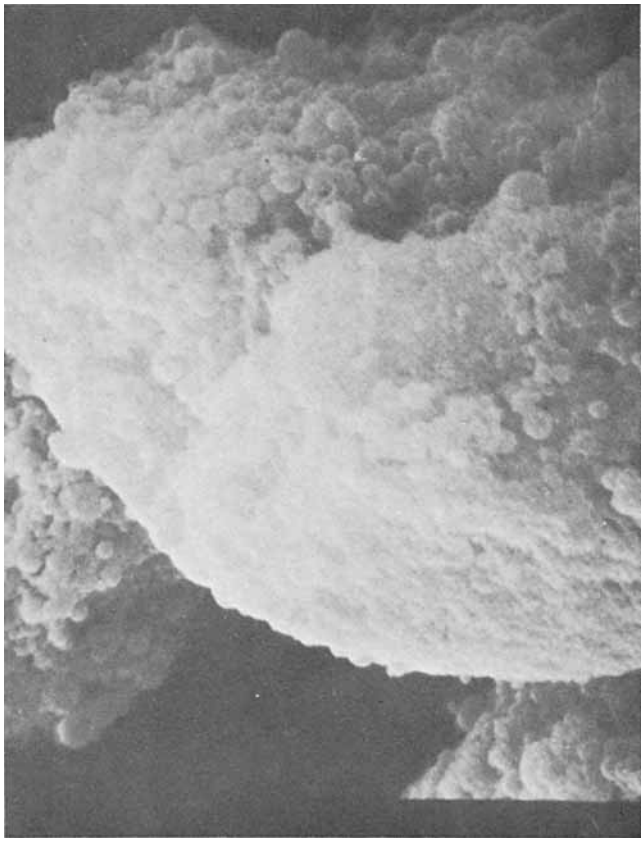

Fig. 8. SEM of fraction 4F: 7,500× showing a broken particle.

3×10^2 rad/sec, the limit of the instrument. Above those frequencies, the data became exceedingly scattered, giving unrealistically high or low values. Probably the response torque is not sinusoidal at the high frequency. However, it is indicated that both the complex viscosity and moduli tended to increase sharply with the increase of frequency.

The data of FF–4C blend series are shown in Figures 12 and 13, with G' and G'' as a function of percentage of the components. When the fine component FF is blended to the coarse 4C, the moduli increase with the concentration of the fine, but no minima were observed. This is contrary to an expectation that the fine particles may fill the interstice of the coarse giving a minimum viscosity and a minimum elastic modulus. While it might occur under the different deformational history such as the steady-state flow, it is not the case here. At about 60/40 ratio of 4C–FF the moduli becomes relatively unaffected by the change of composition. The actual coarse-to-fine ratio estimated from the data of Table I is about 38/62. At both sides of this concentration, moduli depend significantly on the particle size distribution, but the magnitude of dependency decreases with the increasing frequency.

Figures 14–17 are G' and η' of the components and FF–4C blends. The points

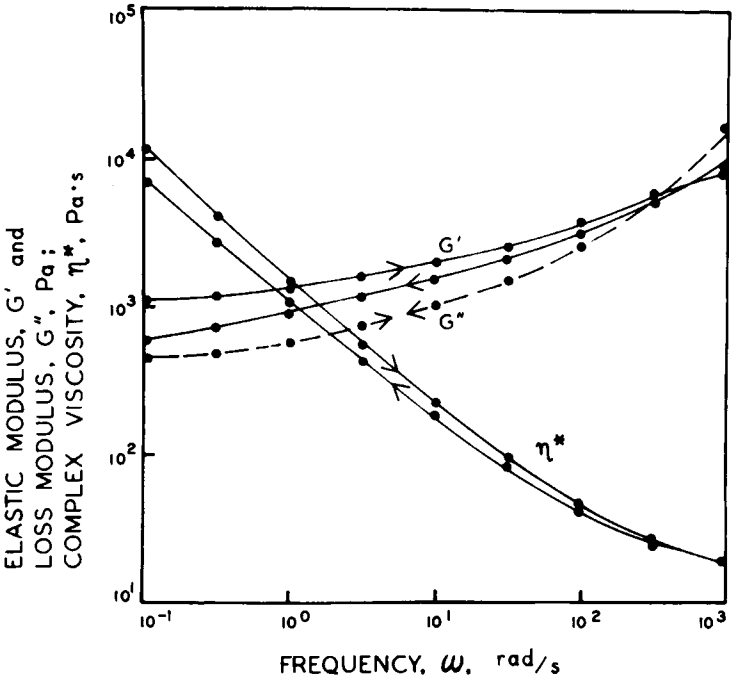

Fig. 9. Nonlinear dynamic behavior of plastisol made from FF fraction. Strain amplitude of 0.0350 for upward sweep, 0.0875 for downward sweep.

are the observed data and the lines are the empirical curve fitting of the following:

$$G' = G'_o + K'\omega^m \tag{1}$$

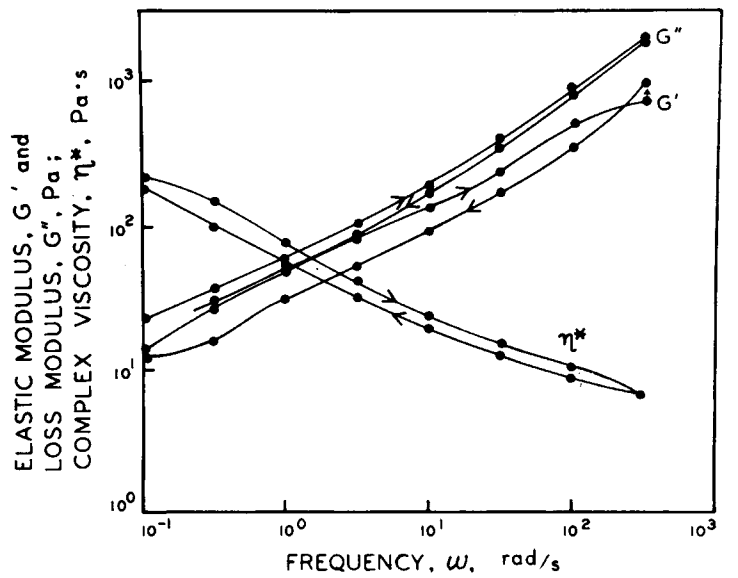

Fig. 10. Nonlinear dynamic behavior of plastisol made from 4C–RF, 75–25, blend. Strain amplitude 0.0350 for upward sweep, 0.0875 for downward sweep.

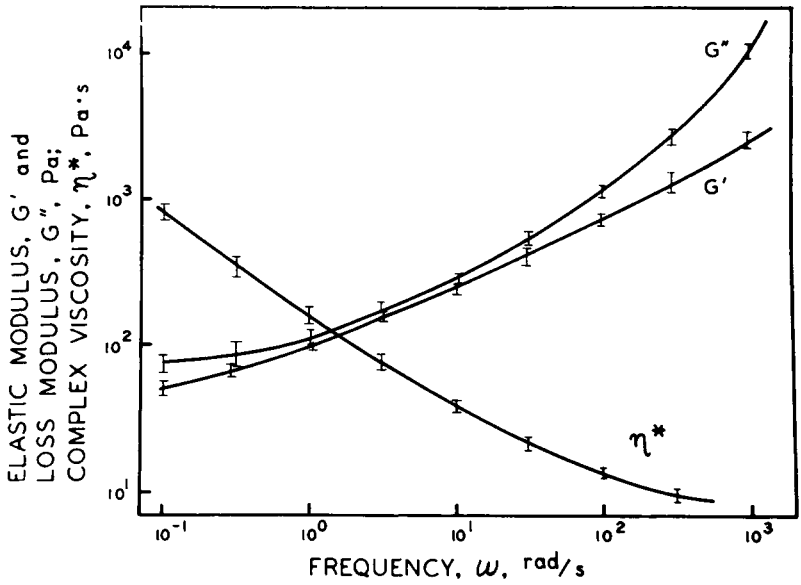

Fig. 11. Reproducibility of dynamic data.

and

$$\eta' = \eta'_\infty + K\omega^{-n} \tag{2}$$

These equations fit very well within the reproducibility of the data including the results not shown here. Six parameters obtained are listed in Table II.

These parameters are related to each other only in very approximate ways. Therefore, we may conclude that there are six independent parameters representing the observed viscosity and elastic modulus.

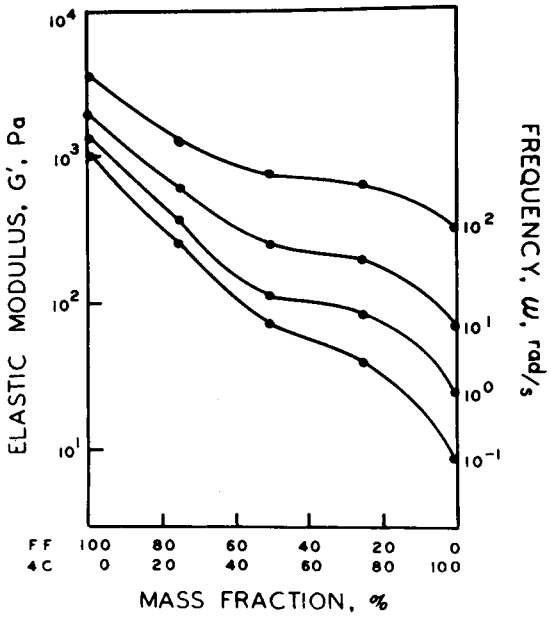

Fig. 12. Dependence of elastic modulus on fine:coarse ratio, FF–4C blends.

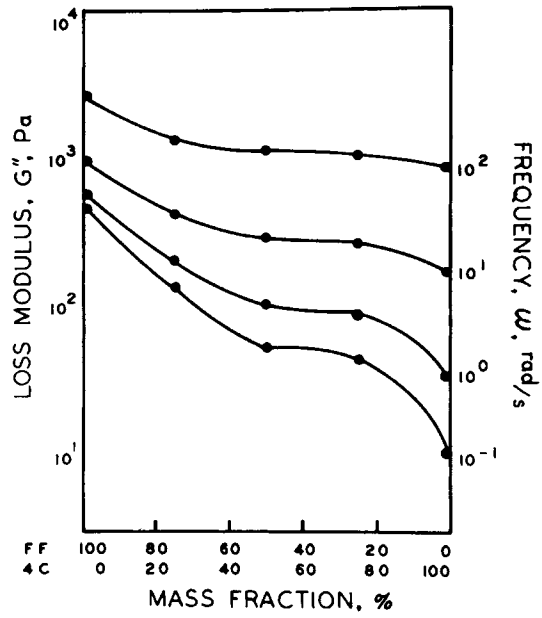

Fig. 13. Dependence of loss modulus on fine:coarse ratio, FF–4C blends.

DISCUSSION

Correlation of Rheological Data With Particle Size Distribution

The rheological behavior may be interpreted if we can relate the rheological parameters of Table II to the particle size distribution. Because the six parameters are independent from each other, each parameter must be related separately to the particle size distribution. For representing the latter, the data of Table I will be used. Because the size of the coarse particles are about the same and the size of fine particles are also about the same, the variables are the mass fractions only; therefore, the mass fraction of the fines, ϕ(f), and that of the ul-

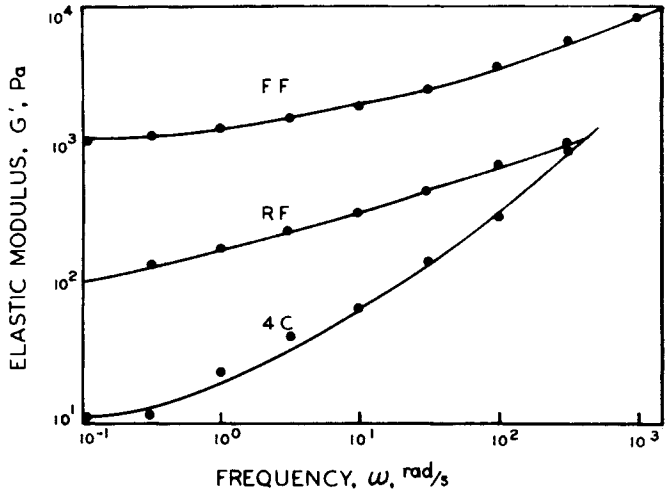

Fig. 14. Elastic modulus frequency curves of blend components, FF, RF, and 4C.

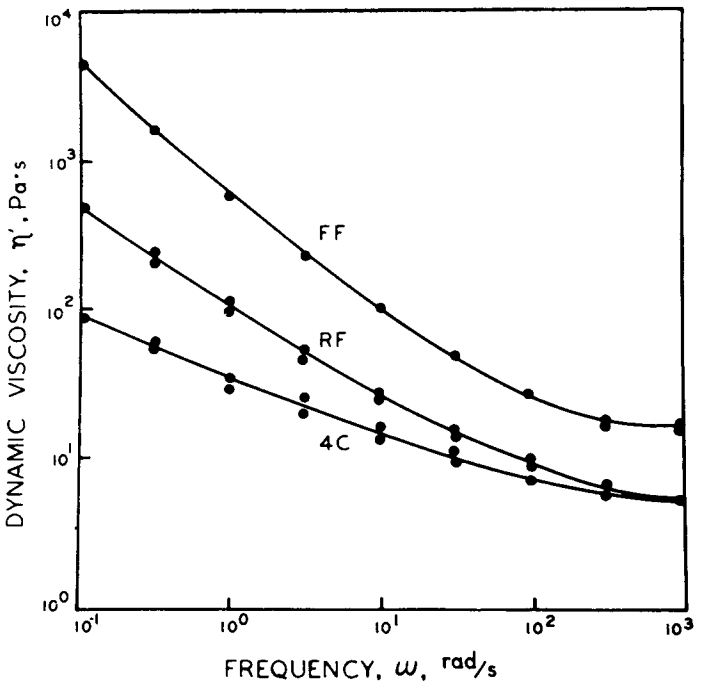

Fig. 15. Dynamic viscosity frequency curves of blend components, FF, RF, and 4C.

trafines, ϕ(uf), will be used to represent the particle size distribution. The observed values of ϕ(uf) are somewhat erratic as shown in Figures 1–3. Therefore, ϕ(uf) of blends were computed from those of the components and used for the correlation.

In Figure 18 G'_o is plotted against mass fraction of the fine and that of the ultrafine in log–log scale. For the observed range, i.e., 28 < ϕ(f) < 73% and 2 <

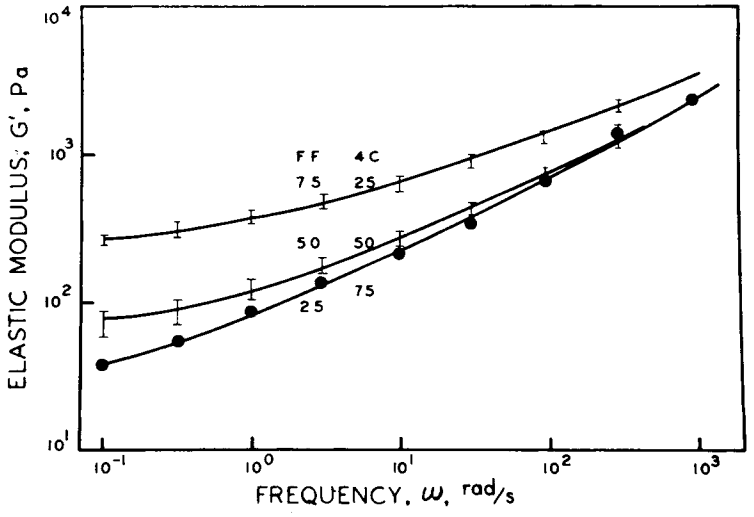

Fig. 16. Elastic modulus frequency curves of FF–4C blends; points are observed data and lines are curve fittings.

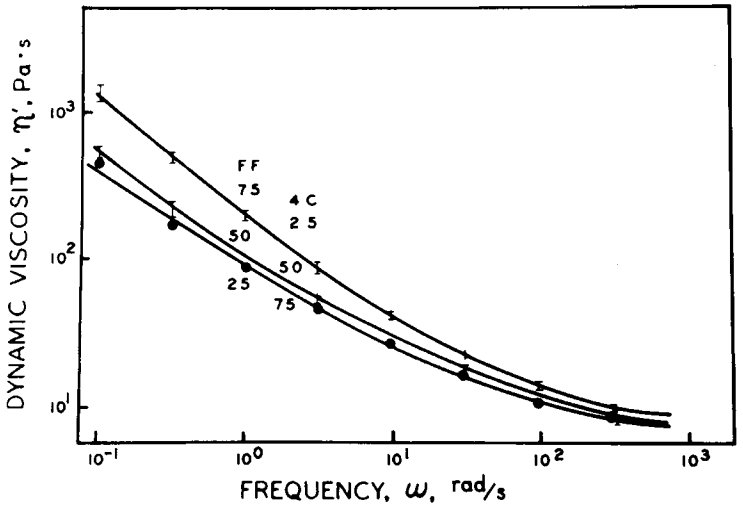

Fig. 17. Dynamic viscosity frequency curves of FF–4C blends, points are observed data and lines are curve fittings.

ϕ(uf) < 24.5%, G'_o increases very steeply with the increase of these fractions. This means that the elastic modulus at the low frequency is significantly increased by the increased amount of the fines and ultrafines.

Figure 19 is a similar plot with K'. This parameter is also similarly dependent on the amount of both the fines and the ultrafines.

The power index, m, decreases sharply with the increased amount of fines and ultrafines (Fig. 20). However, the dependence on the latter is only semiquantitative. The amount of fines seems to have more dominant control on m. That is, when more fines are present, G' increases less with the increasing frequency.

For the viscosity parameter, η'_∞, neither the fine fraction nor the ultrafine

TABLE II
Rheological Parameters

Resin	G', Pa			η Pa·s		
	K'	m	G'	K	n	η'_∞
FF	3.7×10^2	0.432	1.0×10^3	6.00×10^2	0.867	1.5×10^1
FF–RF 25/75	1.87×10^2	0.400	1.4×10^2	1.88×10^2	0.744	6.0×10^0
FF–RF 5/95	1.30×10^2	0.403	7.5×10^1	1.22×10^2	0.700	5.3×10^0
RF	1.30×10^2	0.353	5.0×10^1	1.02×10^2	0.675	4.5×10^0
FF	3.7×10^2	0.432	1.0×10^3	6.0×10^2	0.867	1.5×10^1
FF–4C 75/25	1.72×10^2	0.422	2.0×10^2	2.05×10^2	0.780	8.0×10^0
FF–4C 50/50	6.0×10^1	0.530	6.0×10^1	1.02×10^2	0.667	7.0×10^0
FF–4C 25/75	6.0×10^1	0.530	2.0×10^1	8.5×10^1	0.641	6.5×10^0
4C	9.0×10^0	0.796	9.5×10^0	3.1×10^1	0.456	4.0×10^0
RF	1.30×10^2	0.353	5.0×10^1	1.02×10^2	0.675	4.5×10^0
RF–4C 75/25	7.8×10^1	0.481	4.5×10^1	1.01×10^2	0.638	4.4×10^0
RF–4C 50/50	5.6×10^1	0.500	2.0×10^1	7.7×10^1	0.603	4.3×10^0
RF–4C 25/75	3.35×10^1	0.563	1.4×10^1	5.9×10^1	0.565	4.2×10^0
4C	9.0×10^0	0.796	9.5×10^0	3.1×10^1	0.456	4.0×10^0

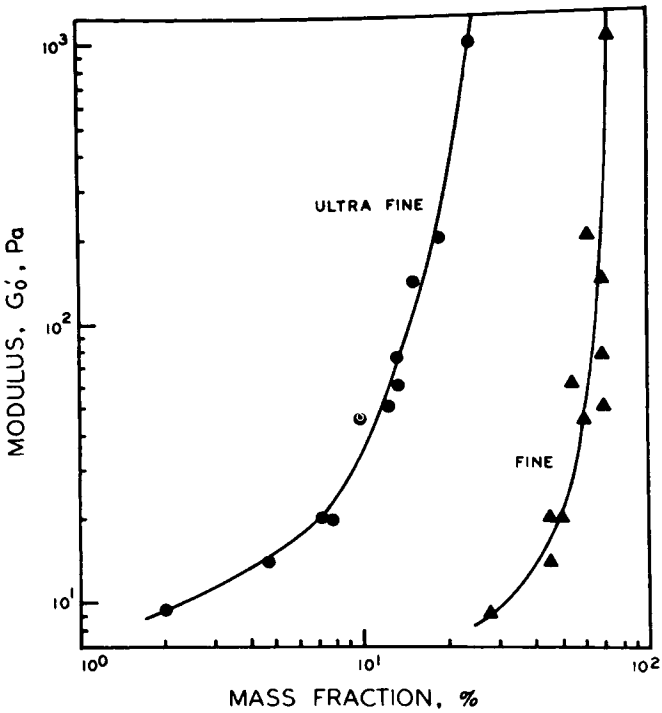

Fig. 18. Dependence of elastic modulus parameter, G'_0 on mass fractions of fine and ultrafine particles.

fraction gave a singular dependence (Fig. 21). As a matter of fact, with 4C–RF blends and components, η'_∞ is almost independent of the amount of the fines and ultrafines, whereas the addition of FF component into either 4C or RF resulted in the increase of η'_∞ value. This implies that the shapes of the particles in 4C and RF may be different. However, optical and electron microscopic observation of particles did not reveal differences in the shapes. The other viscosity parameter, K, is a function of the fraction of the fine and that of the ultrafine (Fig. 22). The latter gives a more quantitative relationship, indicating that the ultrafine exerts a more sensitive control over the parameter K.

The power law index, n, for the viscosity is also dependent on the fraction of the fine and that of the ultrafine. We succeeded to relate quantitatively this parameter to the fraction of the fines and that of the ultrafines (Figs. 23 and 24).

$$n = A + 0.17[\phi(\text{f}) + \phi(\text{uf})] \tag{3}$$

$$A = 0.405 + 1.2\phi(\text{uf}) \tag{4}$$

Combining these two equations, we have

$$n = 0.405 + 0.17\phi(\text{f}) + 1.37\phi(\text{uf}) \tag{5}$$

Mechanism of Rheological Behavior

What mechanism contributes to the observed rheological behavior, is a subject of speculation. However, the microscopic photographs shown in Figure 25 suggest possible mechanisms. These systems are very crowded, approximately

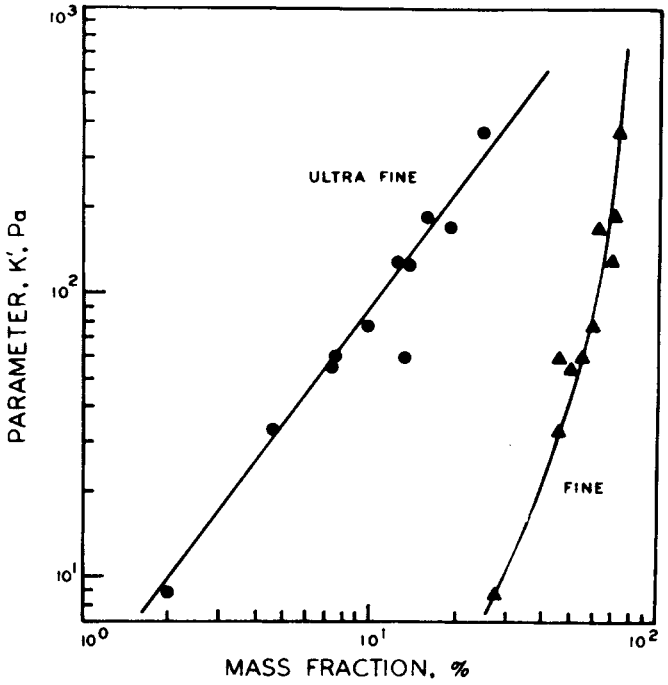

Fig. 19. Dependence of elastic modulus parameter, K', on mass fractions of fine and ultrafine particles.

50 vol % being solid particles. Both the coarse particles and the fine ones in the photographs are in the size ranges listed in Table I.

The coarse particles appear to be placed in the medium containing the fine particles and the plasticizer. The additional disturbances caused by the coarse particles might have been expected to increase both elastic modulus and dynamic viscosity of the medium containing only fines. While this may still be true in some flow conditions, it is not the case here. In the entire frequency range of

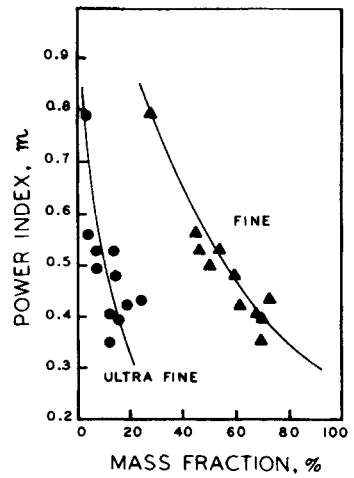

Fig. 20. Dependence of elastic modulus parameter, m, on mass fraction of fine and ultrafine particles.

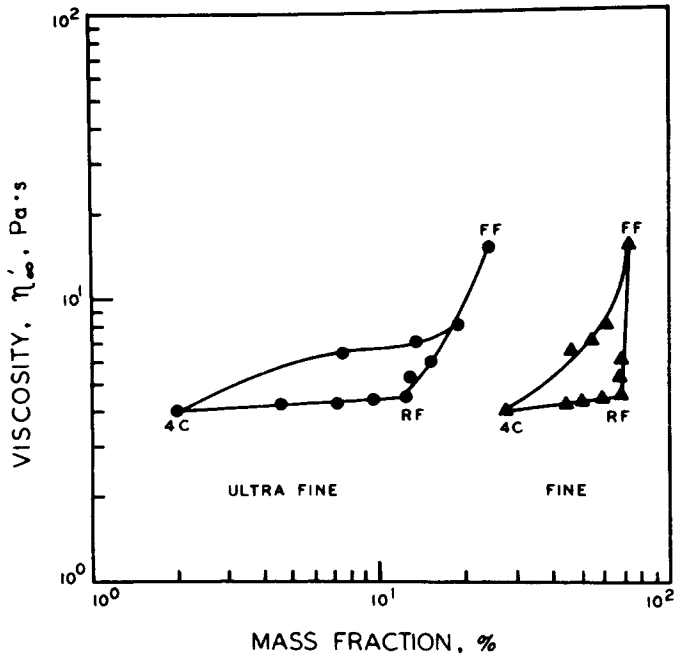

Fig. 21. Dependence of viscosity parameter, η'_∞, on mass fraction of fine and ultrafine particles.

the observation, the elastic modulus actually decreases with the increased amount of the coarse particles. (Figs. 12, 14, 18, and 19).

It appears that a network structure created by the momentary interlocking of particles is responsible for the elastic modulus. Such interlocking depends

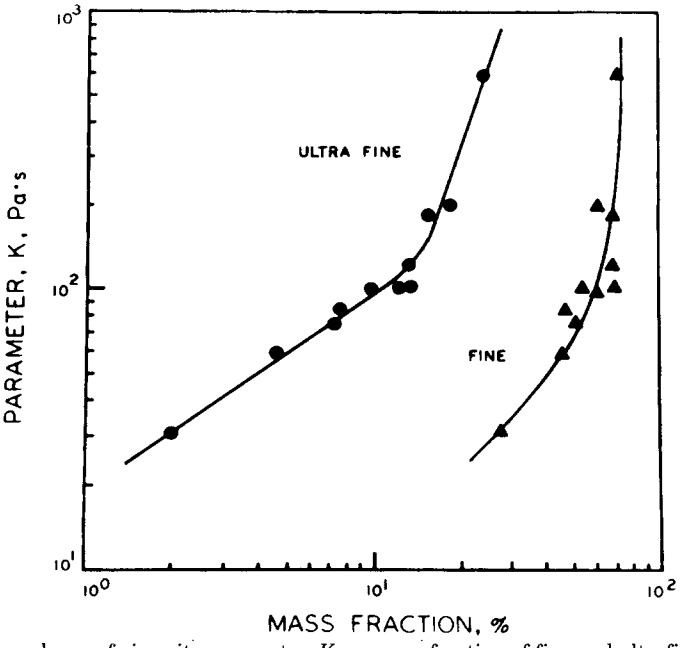

Fig. 22. Dependence of viscosity parameter, K, on mass fraction of fine and ultrafine particles.

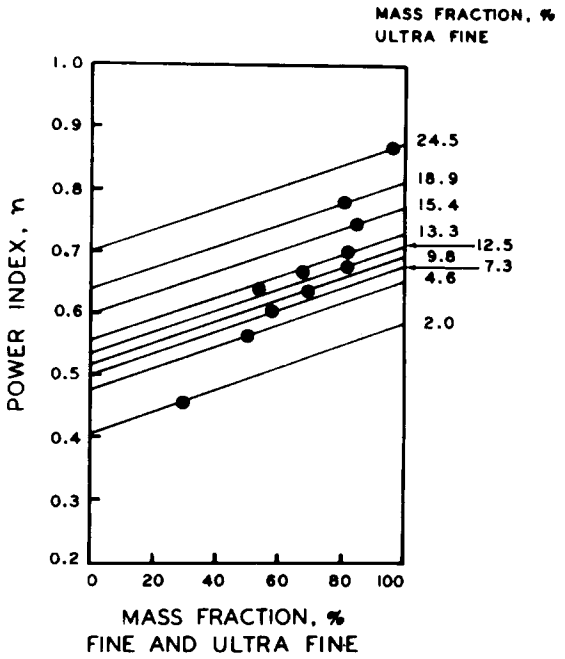

Fig. 23. Dependence of viscosity parameter, n, on mass fraction of fine and ultrafine particles.

upon the contacts between the particles. The probability of having contacts between the neighboring particles depends upon the total surface area of all particles and is inversely related to the average distance between the particles. Therefore, the increased amount of coarse particles decreases the number of contact points.

The elastic modulus increases with the increasing frequency, and the extent of the increase is more marked with the higher amount of course particles (Figs. 12, 14, and 20). The larger particles have more difficulty following the imposed motion, so they contribute to the increased rigidity. At the very high frequencies, perhaps a large fraction of particles become thus immobilized, resulting in a very high modulus.

The dynamic viscosity (and the loss modulus) decreases with the increased

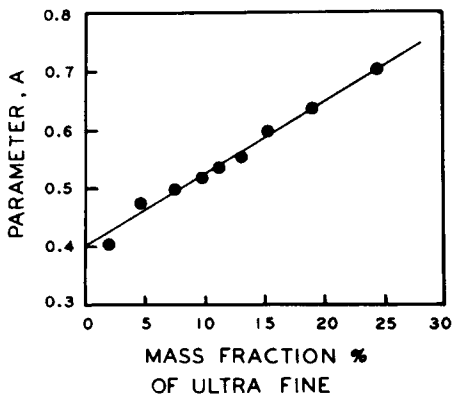

Fig. 24. Dependence of viscosity parameter, A, on mass fraction of ultrafine particles.

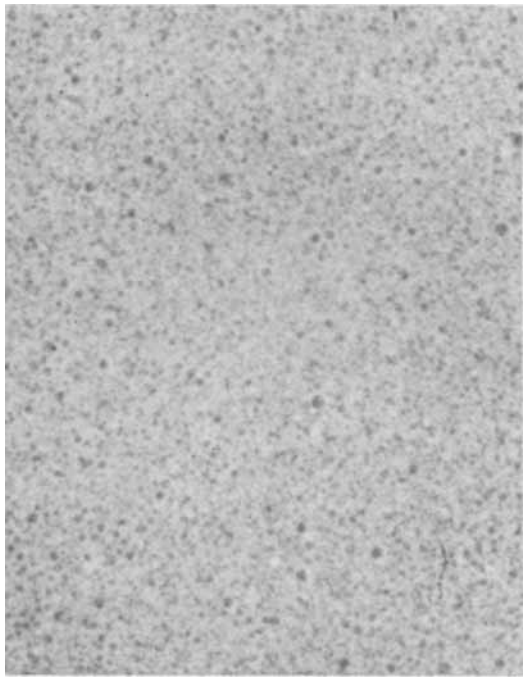

(a) 10 μm

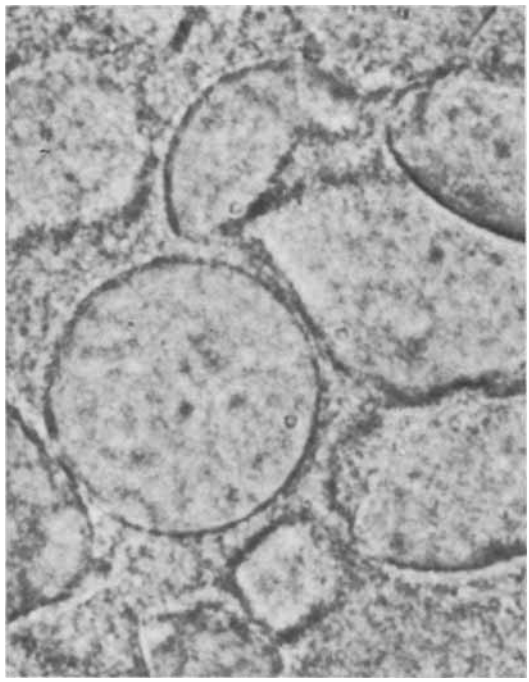

(b) 10 μm

Fig. 25. Optical microphotographs of plastisols made from FF, RF, and 4C fraction: (a) FF, 2,050×; (b) 4C, 2,050×; (c) RF, 210×; (d) 4C, 210×.

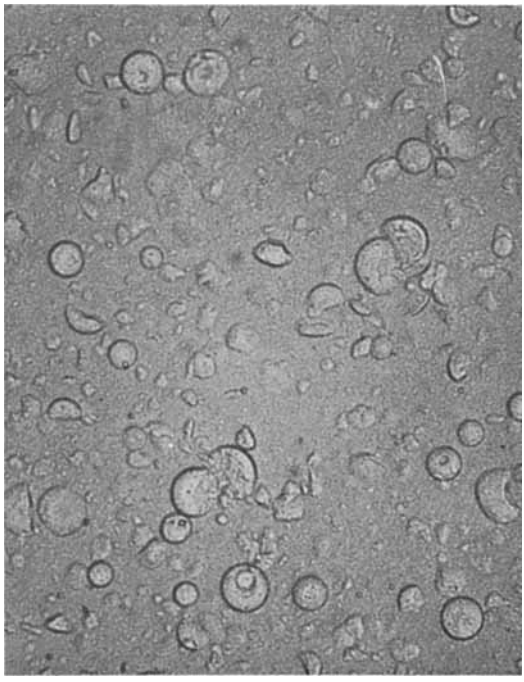

(c) 100 μm

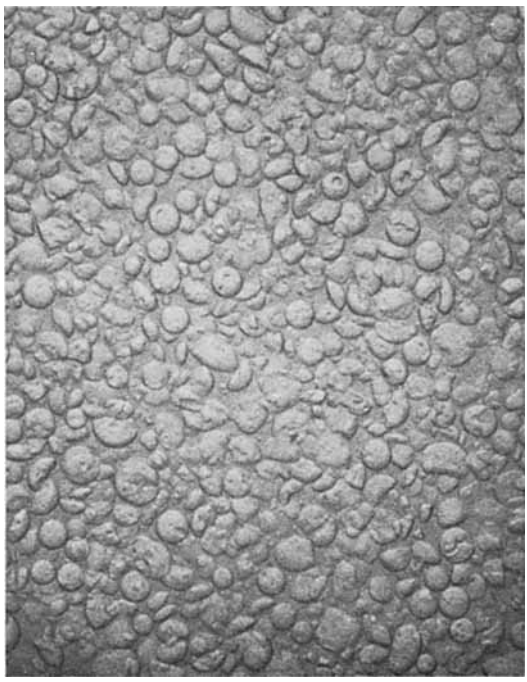

(d) 100 μm

Fig. 25. (*Continued from previous page.*)

amount of coarse particles. (Figs. 13, 15, 21, and 22). The viscous resistance arises from shearing the liquid—i.e., plasticizer, between the opposing surface of the solid particles.

Therefore, the higher viscosity is expected from the increasing total surface area and the decreasing interparticle distances. Thus, the finer particles give the higher viscosity.

The dynamic viscosity decreases with the increasing frequency, and the extent of the decrease is more marked with the higher amount of fine particles (Figs. 13, 15, and 23). Fine particles may become more clustered as the frequency is increased, decreasing the effective surface area and increasing the distance between the shear surfaces.

The rheological models described here must be verified with experimental observation. Then, quantitative treatments of the models may be made.

The optical microscopic observation of particles larger than 0.3 μm did not show any Brownian motion. Although the ultrafine particles are probably undergoing Brownian motion, we do not know if this has any significant influence on the viscoelasticity of the present systems.

Mechanism of Aging

When a PVC plastisol is left at ambient condition, its viscosity increases very rapidly in the beginning and then slowly approaches a steady value. This is called "aging." There are several mechanisms that are postulated to explain the phenomenon. Generally, these may be classified into three categories: dissolution (or swelling), structure formation, and deagglomeration. The present plasticizer system does not dissolve or swell the resin particles, except for the minute amount of very-low-molecular-weight material. The microscopic observations of the plastisols do not reveal any unique structure except that resulting from crowding.

As it has been described, a major change observed during the aging is the deagglomeration. Some of the coarse particles, which are loosely held agglomerates, disintegrated into fine particles. The present work with various blends shows clearly that the increase of the fine fraction results in a very significant increase of viscosity, the magnitude of the increase corresponding to that observed during aging.

CONCLUSIONS

PVC plastisol has been a well-established commercial product for many years. In spite of this, little work has been done to establish a relation among structure, composition, and behavior. For example, rheological studies have been limited to an idealized system of monodispersed sphere or, in the case of commercial systems, were done without reference to the detail of morphology and size distribution of the particles.

In this work we have related the particle size distribution to the dynamic properties of a commercial system. This relationship, together with the microscopic observation of the particle dispersions, provided an interpretation on the plausible mechanisms of the rheological response.

The morphological observation of the particle aggregates, the changes of the

particle size distribution during aging, and the previous rheological study has established that the deagglomeration is the dominant cause of the increase of viscosity during aging.

The authors are grateful to BFGoodrich Chemical Division for permission to publish this work. The optical microscopy was performed by J. D. Isner; the analyses with the scanning electron microscope, courtesy of Case Western Reserve University, were performed by J. A. Davidson and J. D. Isner of BFGoodrich Company. Particle size analyses were done by H. V. Flint. The Rheometrics Mechanical Spectrometer was operated by C. W. Woods.

References

1. (a) "Plastics Engineering Handbook" of the Society of the Plastics Industry, Inc., 4th ed., J. Frados, Ed., Van Nostrand, New York, 1976, p. 365; (b) p. 367; (c) p. 383; (d) p. 369; (e) p. 368.
2. N. Nakajima, D. W. Ward, and E. A. Collins, *J. Appl. Polym. Sci.*, **20,** 1187 (1976).
3. N. Nakajima, D. W. Ward, and E. A. Collins, *Polym. Eng. Sci.*, **19,** 210 (1979).
4. E. A. Collins and J. Hoffman, *Rubber Rev.*, **52,** 676 (1979).
5. R. L. Hoffman, *Trans. Soc. Rheol.*, **16,** 155 (1972).
6. E. A. Collins, J. A. Davidson and C. A. Daniels, *J. Paint Technol.*, **47,** 45 (1975).

Received November 20, 1979
Accepted February 22, 1980